

## Synthesis, X-ray crystallography, vibrational spectroscopy, thermal and DFT studies of (*E*)-6-(4-methylstyryl)-4,5-dihydropyridazin-3(2*H*)-one

Said Daoui<sup>a</sup>, Cemile Baydere<sup>b</sup>, Feride Akman<sup>c</sup>, Fouad El Kalai<sup>a</sup>, Lhassane Mahi<sup>d</sup>, Necmi Dege<sup>b</sup>, Yıldırıay Topcu<sup>e</sup>, Khalid Karrouchi<sup>f,\*</sup>, Noureddine Benchat<sup>a</sup>

<sup>a</sup> Laboratory of Applied Chemistry and Environment (LCAE), Faculty of Sciences, Mohammed I University, 60000 Oujda, Morocco

<sup>b</sup> Department of Physics, Faculty of Arts and Sciences, Ondokuz Mayıs University, Samsun, Turkey

<sup>c</sup> University of Bingöl, Vocational School of Technical Sciences, 12000 Bingöl, Turkey

<sup>d</sup> Moroccan Foundation for Advanced Science, Innovation and Research (Mascir). Department of Nanotechnology. Rabat Design Center, Rue Mohamed Al Jazouli – Madinat Al Irfane Rabat 100, Morocco

<sup>e</sup> Ondokuz Mayıs University, Faculty of Engineering, Chemical Engineering Department, Samsun, Turkey

<sup>f</sup> Laboratory of Analytical Chemistry and Bromatology, Faculty of Medicine and Pharmacy, Mohammed V University, Rabat, Morocco



### ARTICLE INFO

#### Article history:

Received 7 June 2020

Revised 27 August 2020

Accepted 30 August 2020

Available online 31 August 2020

#### Keywords:

Synthesis

Pyridazin-3(2*H*)-one

Crystal structure DFT Hirshfeld surface

Thermal analysis

### ABSTRACT

A novel pyridazin-3(2*H*)-one derivative, (*E*)-6-(4-methylstyryl)-4,5-dihydropyridazin-3(2*H*)-one (**3**) has been synthesized and characterized by FT-IR, UV-vis, <sup>1</sup>H- and <sup>13</sup>C NMR, TGA/DTA thermal analysis and single-crystal X-ray diffraction. Furthermore, the molecular geometry, vibrational frequencies, electronic absorption spectra, chemical shift values, HOMO-LUMO analysis, frontier molecular orbital (FMO) and molecular electrostatic potential (MEP) surface map of the title compound were calculated using DFT/B3LYP method with 6-31+G (d,p) basis set. A comparison among the experimental and calculated results indicates that the vibrational frequencies, maximum electronic absorption wavelengths and chemical shift values are in a good agreement with each other. The intermolecular interactions in the crystal structure were investigated using Hirshfeld surface analysis. TGA/DTA thermal analysis revealed that the title compound is thermostable to its melting point.

© 2020 Elsevier B.V. All rights reserved.

### 1. Introduction

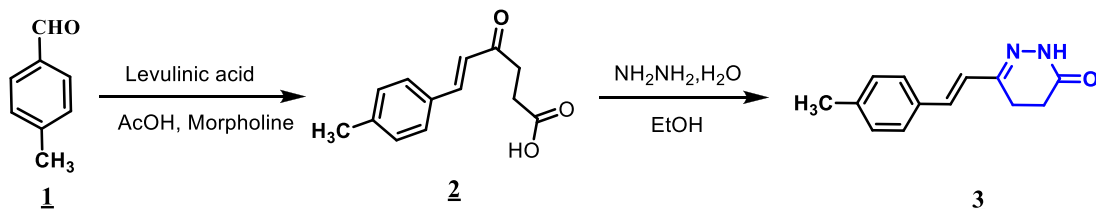
The synthesis of novel pyridazinone derivatives and investigation of their chemical and biological activities have gained more importance in recent years [1,2]. Pyridazinone is an important pharmacophore possessing the wide range of pharmacological applications [3]. Literature survey revealed that substituted pyridazinones have reported to possess biological activities such as anti-HIV, antibacterial, anti-inflammatory, antidepressant, anti-histaminic, antihypertensive, cardiotonic, anticonvulsant, acaracide and herbicidal agents [4–13]. With this background set, the investigation of the structural, electronic and thermodynamic properties of these pyridazin-3(2*H*)-one derivatives are important to know the influence of different substituents on the structures in order to discover the relationship of these substituents with their pharmacological properties. On the other hand, spectroscopic studies and, in particular, electron absorption spectra and vibrational assignments of all the bands observed in the experimental infrared spectra are

of great support in identifying all species in any medium, especially when these studies are combined with theoretical calculations derived from the functional density theory (DFT) [14–22].

In continuation of our studies towards the molecular structures, Hirshfeld surfaces analysis and DFT studies of new pyridazin-3(2*H*)-one derivatives [23–26], we report herein the synthesis of new crystalline derivative i.e., (*E*)-6-(4-methylstyryl)-4,5-dihydropyridazin-3(2*H*)-one (**3**) and, then it was characterized by using FT-IR spectrum in the solid phase, UV-vis, <sup>1</sup>H- and <sup>13</sup>C NMR spectra in DMSO-*d*<sub>6</sub> solution, and single-crystal X-ray diffraction (XRD) (Scheme 1). These experimental studies were accomplished with theoretical DFT calculations by using the functional hybrid B3LYP together with the 6-31+G(d,p) basis set in order to predict the structural, electronic, optical and vibrational properties in the gas phase. Hence, the intermolecular interactions were investigated using Hirshfeld surface analysis and two-dimensional fingerprint plots were also performed. Molecular orbital calculations providing electron-density plots of HOMO and LUMO molecular orbitals and molecular electrostatic potentials (MEP) were also computed both with the DFT/B3LYP/6-31+G(d,p) basis set. In addition, the thermal

\* Corresponding author.

E-mail address: Khalid.karrouchi@um5s.net.ma (K. Karrouchi).

**Scheme 1.** Synthesis of compound 3.

stability of the title compound was evaluated by TGA/DTA thermal analysis.

## 2. Experimental section

### 2.1. General methods

Reactions were checked with TLC using aluminum sheets with silica gel 60 F254 from Merck. Melting points were measured using a Tottoli digital capillary melting point apparatus and are uncorrected. The FT-IR spectrum was recorded with Perkin-Elmer Pargon 1000 PC FT-IR spectrometer over the range 400–4000 cm<sup>-1</sup>. <sup>1</sup>H and <sup>13</sup>C NMR spectra were recorded in DMSO-d<sub>6</sub> solutions on a Bruker Avance III spectrometer at 600 MHz for <sup>1</sup>H NMR and 150 MHz for <sup>13</sup>C NMR. The chemical shifts are expressed in parts per million (ppm). TGA/DTA curves were recorded in a platinum crucible in a pure air atmosphere at a flow rate of 20 mL/min and over-temperature range 0–700 °C with a heating rate of 10 °C/min using Shimadzu thermogravimetric analyzer DTG-60H.

### 2.2. Synthesis

**General procedure for the synthesis of (2):** To a solution of (4 mmol, 0.46 g) of levulinic acid, (3 drops) of morpholine, (9 drops) of glacial acetic acid and in 20 ml of toluene was added (0.48 g, 4 mmol) of 4-methylbenzaldehyde (**1**). The reaction mixture is brought to reflux for 12 h. The completion of the reaction was monitored by TLC. After evaporation of the solvent under reduced pressure, the reaction mixture was cooled and washed with a mixture of acetic acid: water (1: 4). In each case, the precipitate formed was filtered and dried to give the compounds (**2**). Yellow solid, Yield : 79%, m.p = 179–181 °C; <sup>1</sup>H NMR (600 MHz, DMSO-d<sub>6</sub>) δ (ppm): 7.80 (d, *J* = 7.8 Hz, 2H, Ar), 7.61–7.55 (m, 3H, C=CH, Ar), 6.82 (d, *J* = 16.3 Hz, 2H, C=CH), 2.91 (t, *J* = 9.0, 6.0 Hz, 2H, CH<sub>2</sub>), 2.34 (m, 5H, CH<sub>2</sub> and CH<sub>3</sub>); <sup>13</sup>C NMR (150 MHz, DMSO-d<sub>6</sub>) δ (ppm): 199.05 (C=O), 174.44 (COOH), 143.44 (CH=CH), 141.01 (C4 Ar), 131.96 (C4 Ar), 130.03 (CH=CH), 129.75 (C3 Ar), 129.52 (C2 Ar), 35.22 (CH<sub>2</sub>), 28.29 (CH<sub>2</sub>), 21.41 (CH<sub>3</sub>).

**General procedure for the synthesis of (3):** To a mixture of (0.22 g, 1 mmol) of compound (**2**) in 20 ml of ethanol is added (0.044 g, 1.1 mmol) of hydrazine hydrate. The mixture is brought to reflux for four hours. The precipitate was filtered, washed with water, dried and recrystallized from ethanol. Single crystals were obtained by slow evaporation at room temperature. White crystals, Yield : 78%, m.p = 194–196 °C; FT-IR ( $\nu$ (cm<sup>-1</sup>)) : 3305 (NH), 2905–2184 (CH), 1653 (C=O), 1604 (C=N), 1509, 1589 (C=C); <sup>1</sup>H NMR (600 MHz, DMSO-d<sub>6</sub>) δ (ppm): 10.87 (s, 1H, NH), 7.48 (d, *J* = 6.0 Hz, 2H, H-Ar), 7.19 (d, *J* = 6.0 Hz, 2H, H-Ar), 7.01 (d, *J* = 18.0 Hz, 2H, C=CH), 6.84 (d, *J* = 18.0 Hz, 1H, CH=C), 2.77 (t, *J* = 9.0, 6.0 Hz, 2H, CH<sub>2</sub>), 2.38 (t, *J* = 9.0, 6.0 Hz, 2H, CH<sub>2</sub>), 2.31 (s, 3H, CH<sub>3</sub>); <sup>13</sup>C NMR (150 MHz, DMSO-d<sub>6</sub>) δ (ppm): 167.67 (C=O), 151.26 (C6 pyridazinone), 138.52 (C1 Ar), 133.82 (C4 Ar), 133.80 (-CH=CH-pyr), 129.89 (C3 Ar), 127.34 (C2 Ar), 125.87 (-CH=CH-pyr), 26.35 (C6 pyridazinone), 21.36 (C5 pyridazinone), 20.56 (CH<sub>3</sub>).

### 2.3. X-ray crystallography

X-ray single-crystal diffraction for (**3**) was collected at 296 K on a STOE IPDS II diffractometer equipped with an X-ray generator operating at 50 kV and 1 mA, using Cu-K $\alpha$  radiation of wavelength 0.71073 Å. The hemisphere of data was processed using SAINT [27]. The 3D structure was solved by direct methods and refined by full-matrix least squares method on F<sup>2</sup> using the SHELXL program [28,29]. All the non-hydrogen atoms were revealed in the first difference Fourier map and were refined with isotropic displacement parameters. At the end of the refinement, the final difference Fourier map showed no peaks of chemical significance and the final residual was 0.0641. The geometrical calculations were carried out using the program PLATON [30]. The molecular and packing diagrams were generated using Mercury for Windows [31].

### 2.4. Computational details

DFT calculations were made using the Gaussian 09 package program [32] and the results are shown using Gaussview 5.0 [33] molecular visualization program. The applied method are Becke's [34] three parameter hybrid exchange functional with Lee-Yang-Parr correlation functional [35] method (B3LYP) with 6-31+G (d,p) basis set. The frequency calculations show that there is no imaginary frequency and optimized geometry has a true energy minimum. FT-IR and NMR spectra in gas phase are determined by using DFT method at B3LYP/6-31+G (d,p) level of theory and the detailed vibrational assignments were calculated by means of the total energy distribution (TED) method using VEDA 4 program [36].

## 3. Results and discussion

### 3.1. Crystallography studies

A white coloured crystal of dimensions 0.38 × 0.34 × 0.31 mm<sup>3</sup> of compound **3** was chosen for an X-ray diffraction analysis. The single crystal X-ray diffraction data show that it crystallizes in monoclinic system, space group, *P*2<sub>1</sub>/*n*. The details of the crystal data and structure refinement are given in Table 1. In the title compound (Fig. 1a), the dihydropyridazine ring is almost planar, having an r.m.s. deviation of 0.1737 Å for the ring atoms, with the maximum deviation from the ring being 0.2684 (11) Å for the C2 atom; the C3 atom lies -0.2565 (11) Å in of the plane in the opposite direction with the C2 atom. The benzene ring is close to planar with the r.m.s. deviation for the C7–C12 atoms being 0.0066 Å [the maximum deviation from the least-squares plane is 0.0098 (12) Å for the C11 atom]. The dihedral angle between the two mentioned planes is 12.102 (7)°, indicating an approximately planar relationship. The O1=C1 bond length of the pyridazinone carbonyl function is 1.2302 (17) Å and the N1–N2 bond length in the dihydropyridazine ring is 1.3894 (17) Å, both in accordance with values reported for related pyridazinones [37,38].

The main intermolecular interactions in the crystal structure of the title compound are of type N—H...O, C—H•••π (Table 2). N1–H1•••O1 hydrogen bonds between the NH function of the dihy-

**Table 1**  
Crystallographic and refinement data for compound (3).

CCDC Deposition Number	2,006,774
Chemical formula	C <sub>13</sub> H <sub>14</sub> N <sub>2</sub> O
M <sub>r</sub>	214.26
Crystal system, space group	Monoclinic, P2 <sub>1</sub> /n
Temperature (K)	296
a, b, c (Å)	7.4873 (5), 13.0255 (7), 12.1238 (8)
β (°)	107.108 (5)
V (Å <sup>3</sup> )	1130.07 (13)
Z	4
Radiation type	Mo Kα
μ (mm <sup>-1</sup> )	0.08
Crystal size (mm)	0.38 × 0.34 × 0.31
<b>Data collection</b>	
Diffractometer	STOE IPDS 2
Absorption correction	Integration (X-RED32; Stoe & Cie, 2002)
T <sub>min</sub> , T <sub>max</sub>	0.971, 0.990
No. of measured, independent and observed [I > 2σ(I)] reflections	7905, 2214, 1718
R <sub>int</sub>	0.032
(sin θ/λ) <sub>max</sub> (Å <sup>-1</sup> )	0.617
<b>Refinement</b>	
R[F <sup>2</sup> > 2σ(F <sup>2</sup> )], wR(F <sup>2</sup> ), S	0.043, 0.114, 1.04
No. of reflections	2214
No. of parameters	147
H-atom treatment	H-atom parameters constrained
Δρ <sub>max</sub> , Δρ <sub>min</sub> (e Å <sup>-3</sup> )	0.14, -0.14

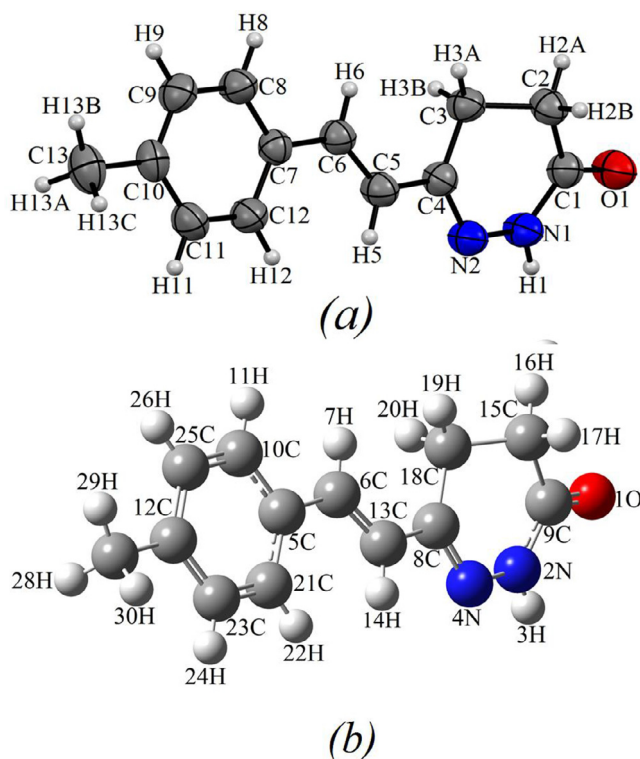


**Fig. 1.** The molecular structure of the title compound: a) ORTEP drawn at the 50% probability level. b) Optimized DFT/6-31+G (d,p) level.

**Table 2**  
Hydrogen-bond geometry (Å, °).

D—H•••A	D—H	H•••A	D•••A	D—H•••A
N1—H1•••O1 <sup>i</sup>	0.872 (19)	2.026 (19)	2.8928 (17)	172.6 (16)
C2—H2B•••Cg2 <sup>ii</sup>	0.97	2.72	3.6598 (17)	162.0

Symmetry codes: (i) -x + 1, -y, -z + 1; (ii) -x + 3/2, y + 1/2, -z + 1/2

dihydropyridazine ring and the carbonyl O atom generate centrosymmetric dimers with an R<sub>2</sub><sup>2</sup>(8) ring motif. The two types of hydrogen bonding results in the formation of layers parallel (200). In the crystal, adjacent molecules are linked via C2—H2B•••Cg2 (3/2-x, 1/2+y, 1/2-z; Cg2 is the centroid of the C7–C12 benzene ring) interactions, forming chains along [030] (Table 2, Fig. 2). Notable π•••π interactions are not observed.

### 3.2. Optimized geometry

The optimized geometry of (E)-6-(4-methylstyryl)-4,5-dihydropyridazin-3(2H)-one (3) is presented in Fig. 1b. The optimized geometrical parameters of (E)-6-(4-methylstyryl)-4,5-dihydropyridazin-3(2H)-one (3) in gas phase by using the B3LYP/6-31+G (d,p) method are summarized in Table 3. These geometrical parameters are compared in the same table with the corresponding experimental ones determined. The deviation values are also included in that table to evaluate the differences between theoretical and experimental results. Hence, good correlations are observed for bond lengths and angles with deviation values between 0 and 0.001 Å for bond lengths and of 0 and 0.05° for bond angles. The higher deviations are clearly observed for bond angles H1—N1—C1 and H1—N1—N2 with deviation values 3.42 and 3.96°, respectively. The good correlations evidenced in the bond lengths and angles, indicate that the optimized structure of compound (3) in gas phase by using the B3LYP/6-31+G (d,p) method can be used to perform the vibrational analysis.

From the results we can say that, the DFT/B3LYP functional method estimated the bond lengths, bond angles and dihedral angles in good agreement with literature [39–43].

### 3.3. FT-IR study

The experimental and theoretical FT-IR spectra of the title compound are presented in Fig. 3. All vibrational assignments calculated by means of TED and the selected significant frequency vibrations are listed in Table 4.

#### 3.3.1. N—H vibrations

The N—H stretching vibrations are generally appears in the region 3500–3000 cm<sup>-1</sup> [44]. This absorption is highly influenced

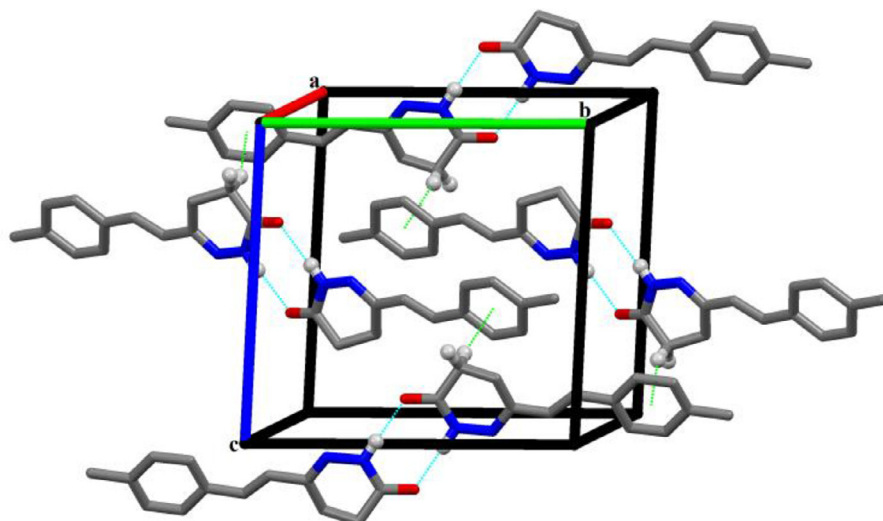


**Fig. 2.** A view along the *a* axis of the crystal structure of the title compound. Blue dashed lines symbolize intermolecular N–H $\bullet\bullet\bullet$ O hydrogen bonds; C–H $\bullet\bullet\bullet$  $\pi$  interactions are shown as green dashes lines.

**Table 3**

Experimental and theoretical bond lengths and angles for compound (3). The crystallographic atom-labeling scheme was followed.

	XRD	DFT	$\Delta$ (Theor-Exp)		XRD	DFT	$\Delta$ (Theor-Exp)
Bond length (Å)				Bond length (Å)			
O1-C1	1.230(2)	1.230	0	C10-C11	1.382(2)	1.382	0
N1-C1	1.342(2)	1.342	0	C10-C13	1.506(2)	1.506	0
N1-N2	1.390(2)	1.389	-0.001	C5-H5	0.930	0.930	0
N1-H1	0.872(2)	0.860	-0.012	C2-C3	1.516(2)	1.515	-0.001
N2-C4	1.286(2)	1.287	0.001	C2-H2A	0.970	0.970	0
C7-C8	1.391(2)	1.391	0	C2-H2B	0.970	0.969	-0.001
C7-C12	1.392(2)	1.391	-0.001	C3-H3A	0.970	0.970	0
C7-C6	1.463(2)	1.462	-0.001	C3-H3B	0.970	0.970	0
C6-C5	1.327(2)	1.327	0	C12-C11	1.374(2)	1.374	0
C6-H6	0.930	0.929	-0.0001	C12-H12	0.930	0.930	0
C4-C5	1.451(2)	1.450	-0.001	C11-H11	0.930	0.930	0
C4-C3	1.494(2)	1.493	-0.001	C9-H9	0.930	0.930	0
C1-C2	1.490(2)	1.490	0	C13-H13A	0.960	0.960	0
C8-C9	1.382(2)	1.381	-0.001	C13-H13B	0.960	0.960	0
C8-H8	0.930	0.930	0	C13-H13C	0.960	0.960	0
C10-C9	1.379(2)	1.378	-0.001				
Bond angle (°)				Bond angle (°)			
N2-N1-C1	126.81	126.85	0.04	C1-C2-H2A	109.40	109.39	-0.01
H1-N1-C1	120.00	116.58	-3.42	H2A-C2-C3	109.40	109.39	-0.01
H1-N1-N2	112.60	116.56	3.96	C1-C2-H2B	109.40	109.40	0
N1-N2-C4	116.66	116.66	0	H2B-C2-C3	109.40	109.40	0
C8-C7-C12	116.79	116.77	-0.02	H2A-C2-H2B	108.00	108.01	0.01
C6-C7-C8	119.58	119.56	-0.02	C4-C3-C2	110.33	110.36	0.03
C6-C7-C12	123.64	123.65	0.01	C4-C3-H3A	109.60	109.57	-0.03
C7-C6-C5	126.54	126.52	-0.02	C2-C3-H3A	109.60	109.57	-0.03
H6-C6-C5	116.70	116.73	0.03	C4-C3-H3B	109.60	109.58	-0.02
C7-C6-H6	116.70	116.74	0.04	C2-C3-H3B	109.60	109.58	-0.02
N2-C4-C5	115.26	115.22	-0.04	H3A-C3-H3B	108.10	108.11	0.01
N2-C4-C3	122.40	122.39	-0.01	C7-C12-C11	121.07	121.08	0.01
C5-C4-C3	122.30	122.34	0.04	H12-C12-C11	119.50	119.45	-0.05
O1-C1-N1	121.35	121.35	0	C7-C12-H12	119.50	119.45	-0.05
O1-C1-C2	123.73	123.74	0.01	C10-C11-C12	121.86	121.84	-0.02
N1-C1-C2	114.92	114.88	-0.04	C12-C11-H11	119.10	119.07	-0.03
C7-C8-C9	121.77	121.76	-0.01	C10-C11-H11	119.10	119.08	-0.02
H8-C8-C9	119.10	119.11	0.01	C8-C9-C10	120.91	120.91	0
C7-C8-H8	119.10	119.11	0.01	C10-C9-H9	119.50	119.54	0.04
C11-C10-C9	117.58	117.57	-0.01	C8-C9-H9	119.50	119.54	0.04
C9-C10-C13	121.39	121.39	0	C10-C13-H13A	109.50	109.46	-0.04
C11-C10-C13	121.03	121.03	0	C10-C13-H13B	109.50	109.46	-0.04
C6-C5-C4	126.07	126.03	-0.04	H13A-C13-H13B	109.50	109.46	-0.04
C6-C5-H5	117.00	116.98	-0.02	C10-C13-H13C	109.50	109.47	-0.03
C4-C5-H5	117.00	116.98	-0.02	H13A-H13-H13C	109.50	109.47	-0.03
C1-C2-C3	111.18	111.17	-0.01	H13B-C13-H13C	109.50	109.47	-0.03

**Table 4**

Calculated frequencies, relative intensities, observed IR frequencies, and probable assignments of the compound (3).

$\nu_{(DFT)}$ (cm $^{-1}$ )	DFT /B3LYP (cm $^{-1}$ )		Assignments, TED (<10%)	$\nu_{(DFT)}$ (cm $^{-1}$ )	DFT /B3LYP (cm $^{-1}$ )		$\nu_{(IR)}$ (cm $^{-1}$ )	Assignments, TED (<10%)
	$\nu_{(IR)}$ (cm $^{-1}$ )	$I_{IR}$			$I_{IR}$	$\nu_{(IR)}$ (cm $^{-1}$ )		
3622.4	48.29	3305	$\nu$ NH (100)	1270.31	70.46	1256	$\delta$ HCC (16) + $\delta$ NN (13)	
			$\nu$ CH (11) + $\nu$ CH (84)					
3198.52	13.14	24.04	$\nu$ CH (42) + $\nu$ CH (55)	1239.61	44.79	4.44	$\nu$ CC (16)	
			$\nu$ CH (45)					
3190.66	14.22	3184	$\nu$ CH (45)	1235.43	21.07	1210	$\delta$ HCC (14) + $\delta$ HCC (18) + $\delta$ HCC (21) + $\delta$ HCC (13)	
			$\nu$ CH (45)					
3177.05	9.84	16.98	$\nu$ CH (45)	1209.23	21.95	1183	$\delta$ HCC (22) + $\delta$ HCC (14) + $\tau$ HCCC (12)	
			$\nu$ CH (73)					
3173.6	7.88	7.93	$\nu$ CH (47) + $\nu$ CH (40)	1173.19	23.71	1153	$\nu$ NN (23)	
			$\nu$ CH (93)					
3171.05	18.40	18.40	$\nu$ CH (80)	1148.64	33.39	4.81	$\delta$ HCC (13)	
			$\nu$ CH (93)					
3166.97	14.13	14.13	$\nu$ CH (93)	1142.83	1107	1041	$\delta$ HCH (10) + $\tau$ HCCC (24)	
			$\nu$ CH (93)					
3128.57	7.88	7.93	$\nu$ CH (93)	1061.07	1.79	1041	$\tau$ CNNC (14) + $\tau$ CCNC (21)	
			$\nu$ CH (80)					
3120.14	15.52	15.44	$\nu$ CH (52)	1040.63	3.76	1017	$\delta$ CCC (20)	
			$\nu$ CH (88)					
3097.17	15.44	15.44	$\nu$ CH (47) + $\nu$ CH (18) + $\nu$ CH (35)	1009.19	12.46	995	$\delta$ NNC (19) + $\delta$ NNC (18) + $\tau$ HCCN (11)	
			$\nu$ CH (91)					
3034.08	11.15	11.15	$\nu$ OC (82)	977.26	0.01	973	$\nu$ CC (15) + $\delta$ NNC (11)	
			$\nu$ CC (40) + $\delta$ HCC (14)					
3014.41	766.68	766.68	$\nu$ CC (28)	967.39	69.67	960	$\tau$ HCCC (17)	
			$\nu$ CC (41) + $\nu$ CC (40)					
1764.39	109.48	109.48	$\nu$ CC (18)	961.27	1.01	960	$\delta$ CCN (14) + $\delta$ CCN (10)	
			$\nu$ CC (18)					
1699.33	18.46	18.46	$\nu$ NC (41) + $\nu$ CC (40)	886.57	0.25	799	$\tau$ NCCC (13)	
			$\nu$ CC (18)					
1659.45	13.20	13.20	$\delta$ HCC (16) + $\delta$ HCC (17)	821.29	49.61	750	$\tau$ HCCC (21) + $\tau$ HCCC (25) + $\tau$ HCCC (27)	
			$\delta$ HCH (17) + $\delta$ HCH (17)					
1604.03	13.83	24.99	$\delta$ HCH (41)	795.32	4.13	750	$\tau$ HCCC (18) + $\tau$ HCCC (18) + $\tau$ HCCC (15)	
			$\delta$ HCH (74) + $\delta$ HCH (13)					
1549.97	11.02	1509	$\delta$ NC (13) + $\nu$ CC (32) + $\delta$ CCN (12)	765.04	2.55	707	$\delta$ CCC (16)	
			$\delta$ CCC (16)					
1498.42	7.27	7.27	$\delta$ HCH (41)	717.65	1.09	707	$\tau$ CCCC (14)	
			$\delta$ HCH (74) + $\delta$ HCH (13)					
1490.25	9.45	8.34	$\delta$ HCH (73)	655.47	1.71	625	$\delta$ CCC (17) + $\delta$ CCC (20)	
			$\delta$ HNN (54)					
1453.35	13.26	14.93	$\nu$ CC (16) + $\delta$ HNN (16)	607.2	30.98	590	$\tau$ HNNC (23)	
			$\nu$ CC (16) + $\delta$ HNN (16)					
1448.38	0.06	1.57	$\delta$ HCH (45) + $\delta$ HCH (25) + $\delta$ HCH (22)	590.5	34.55	517	$\delta$ OCN (15) + $\tau$ CCCC (12)	
			$\nu$ CC (15) + $\delta$ HCC (17)					
1420.79	2.05	2.05	$\delta$ HCC (21)	518.87	14.23	498	$\delta$ OCN (12) + $\tau$ CCCC (12)	
			$\nu$ CC (19) + $\delta$ HCC (30)					
1354.11	28.58	28.58	$\delta$ HCC (10) + $\tau$ HCCC (18) + $\tau$ HCCN (19)	449.92	8.04	457	$\delta$ CCC (11)	
			$\delta$ HCC (22)					
1343.97	26.92	216.41	$\delta$ HCC (21)	418.1	0.94	424	$\tau$ CCCC (23) + $\tau$ CCCC (12)	
			$\nu$ CC (12)					
1338.27	1308.37	1308.37	$\delta$ HCC (22)	410.94	5.01	470	$\delta$ OCN (11) + $\tau$ HCCN (12)	
			$\nu$ IR (1291)					

 $\nu$ ; stretching.  $\delta$ ; bending.  $\tau$ ; torsion vibrations.

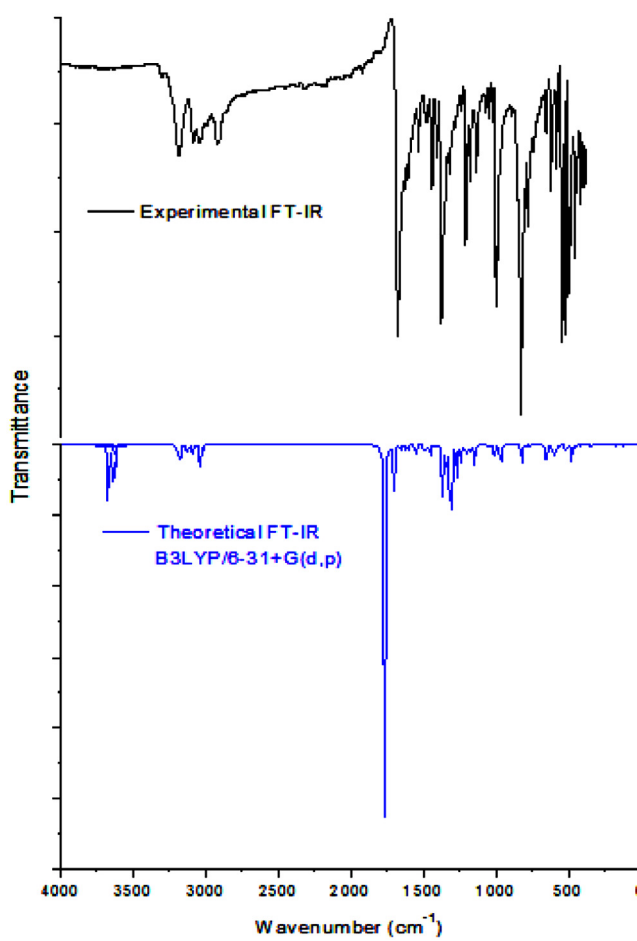


Fig. 3. Comparative representations of FT-IR spectra for (3).

by chemical environment, mainly when NH group are involved in hydrogen bonding. This can occur within the same molecule (intramolecular H bonding) or with neighboring molecules (intermolecular H bonding) [45]. The NH stretching band in pyridazin-3(2H)-one is reported at 3337 cm<sup>-1</sup> by Bahçeli et al. [46] and at by Soliman et al. [47]. In the IR spectrum of **3**, we observed a sharp band of weak intensity at 3305 cm<sup>-1</sup>, assigned to  $\nu_{\text{NH}}$  absorption and the calculated value is 3622 cm<sup>-1</sup>. The difference observed between theoretical and experimental values concerning  $\nu_{\text{NH}}$  is due to the fact that the N1—H1 $\cdots$ O1<sup>i</sup> hydrogen bond was not taken into account in our calculations: intermolecular H bonds were purposely omitted since it is usually employed, for computation, a single molecule (gas phase) approach. Soliman et al. [47] reported the N-H in-plane and out-of-plane deformation vibrations in pyridazin-3(2H)-one at 1393 and 652 cm<sup>-1</sup>, respectively. In this case, the bands observed at 1379 and 590 cm<sup>-1</sup> in IR spectrum are assigned as these modes. These deformation vibrations are calculated at 1453 and 607 cm<sup>-1</sup>, respectively.

### 3.3.2. C—H vibrations

The C—H stretching vibrations of aromatic rings give rise to bands in the region 3200–3000 cm<sup>-1</sup> in aromatic compounds [44,48–50]. Here, the calculated stretching vibrations in the range of 3198–3166 cm<sup>-1</sup> are attributed to C—H stretching vibration in benzene ring. The scaled signals at 3128, 3097, 3041 and 3014 cm<sup>-1</sup> are attributed to the C—H ( $\text{sp}^2$  and  $\text{sp}^3$ ) stretching vibrations in pyridazin-3(2H)-one ring and the signals at 3120, 3087 and 3034 cm<sup>-1</sup> are attributed to the stretching vibrations of the

$-\text{CH}_3$  substituent group connected to benzene ring. Experimentally, the series of IR bands in the range 3184–2905 cm<sup>-1</sup> were assigned as CH ( $\text{sp}^2$  and  $\text{sp}^3$ ) stretching modes of the 4-methylbenzyl and pyridazin-3(2H)-one rings.

In para substituted benzene, the C—H in-plane bending or deformations vibrations are observed in the region 1400–1000 cm<sup>-1</sup> and are usually of medium to weak intensity [44,48–50]. Here, some bands due to C—H in-plane bending vibration in the title compound interact somewhat with other vibrations and they can be assigned to the bands in the region between 1414 and 1041 cm<sup>-1</sup>. The DFT calculations give these modes in the range 1549–1142 cm<sup>-1</sup>.

The out-of-plane C—H deformations are observed between 900 and 600 cm<sup>-1</sup> [48–50]. Generally the CH out-of-plane deformations typical for para substituted benzenes are assigned in the  $840 \pm 50$  cm<sup>-1</sup> region [51]. In the present work, these vibration modes can be associated to the IR bands observed between 995 and 707 cm<sup>-1</sup>, experimentally and at 1009, 977, 961, 842 and 821 cm<sup>-1</sup>, theoretically.

### 3.3.3. Carbonyl C=O vibrations

The stretching mode C=O is generally one of the most intense peak in an infrared spectrum, it appears in a region 1800–1600 cm<sup>-1</sup> [44]. For pyridazin-3(2H)-one, this mode was reported at 1674 cm<sup>-1</sup> by Bahçeli et al. [46] and at 1664 cm<sup>-1</sup> by Soliman et al. [47]. In our study, the C=O stretching mode in the pyridazin-3(2H)-one is assigned to the intense band at 1653 cm<sup>-1</sup>. This mode was computed at 1764 cm<sup>-1</sup>.

### 3.3.4. C=N and N-N vibrations

Dede et al. [52] reported the C=N stretching vibrations at 1616 cm<sup>-1</sup> in pyridazin-3(2H)-one. For the title compound, the bands observed at 1604 cm<sup>-1</sup> are assigned as C=N stretching mode, which is comparable to theoretical value at 1621 cm<sup>-1</sup>. On the other hand, the N-N stretching mode has been reported at 1131 cm<sup>-1</sup> in bromopyrazone [53]. In the present case, the band observed at 1153 cm<sup>-1</sup> is assigned as N-N stretching vibration in pyridazin-3(2H)-one, which is found to be in good agreement with the calculated value 1148 cm<sup>-1</sup>.

### 3.3.5. C=C and C—C vibrations

The aromatic C=C stretching vibrations of vinyl and phenyl ring are very much important and occur in the region 1200–1650 cm<sup>-1</sup> [48–50,53]. For the studied molecule, the calculated bands at 1699 and 1659 cm<sup>-1</sup> attributed to C=C stretching vibration in vinyl group and benzene ring, respectively. These vibration modes were observed at 1509 and 1582 cm<sup>-1</sup>, experimentally. Moreover, the C—C in plane and out of plane bending vibrations are reported at 673 and 580 cm<sup>-1</sup>, respectively [54]. The in-plane and out-of-plane ring deformations of title compound are observed in the region below 750 and 470 cm<sup>-1</sup>.

### 3.4. <sup>1</sup>H and <sup>13</sup>C NMR chemical shifts

The experimental and the theoretical <sup>1</sup>H and <sup>13</sup>C NMR chemical shifts of the title compound were obtained by using DMSO-*d*<sub>6</sub> as solvent. The predicted ones were obtained at B3LYP/6-31+G(d,p) level using CPCM model and GIAO method and the obtained results and experimental values were given in Table 5. The proton NMR spectrum of compound **3** displayed a singlet at  $\delta = 2.31$  ppm due to H28, H29 and H30 protons of methyl (CH<sub>3</sub>) group. Their corresponding ones are underestimated by 2.93, 2.33 and 2.83 ppm. The chemical shifts of H16, H17, H19 and H20 protons of methylene (-CH<sub>2</sub>-) group of pyridazone appear as two triplets at  $\delta = 2.38$  and 2.77 ppm. The chemical shifts of H7 and H14 protons of vinyl (-CH=CH-) group appear as two doublets at  $\delta = 6.84$  and

**Table 5**  
The experimental and computed  $^1\text{H}$ - and  $^{13}\text{C}$  NMR chemical shifts, all values in ppm of the compound **3**.

Atoms	Chemical shifts of hydrogen atoms		Atoms	Chemical shifts of carbon atoms	
	Exp.	Theo.		Exp.	Theo.
<b>3-H</b>	10.87	8.39	<b>9-C</b>	167.67	153.99
<b>11-H</b>	7.48	8.24	<b>8-C</b>	151.21	139.36
<b>7-H</b>	7.01	8.02	<b>12-C</b>	133.82	128.25
<b>26-H</b>	7.19	7.67	<b>5-C</b>	138.52	120.33
<b>24-H</b>	7.19	7.58	<b>21-C</b>	127.34	118.79
<b>22-H</b>	7.48	7.54	<b>6-C</b>	125.87	118.55
<b>14-H</b>	6.84	7.04	<b>23-C</b>	129.89	116.27
<b>20-H</b>	2.38	3.08	<b>25-C</b>	129.89	116.01
<b>28-H</b>	2.31	2.93	<b>10-C</b>	127.34	109.70
<b>19-H</b>	2.38	2.85	<b>13-C</b>	133.80	108.06
<b>30-H</b>	2.31	2.83	<b>18-C</b>	21.36	20.04
<b>17-H</b>	2.77	2.74	<b>15-C</b>	26.35	19.81
<b>16-H</b>	2.77	2.52	<b>27-C</b>	20.56	12.09
<b>29-H</b>	2.31	2.33			

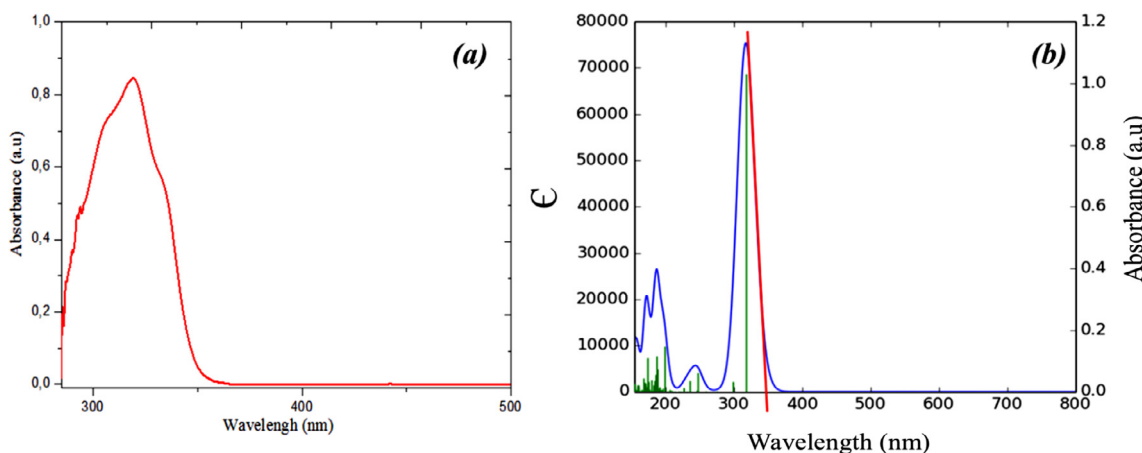


**Fig. 4.** Experimental (a) and simulated (b) UV-vis spectrum of the compound **3**.

7.01 ppm. Indeed, the predicted chemical shifts of these protons are obtained at  $\delta = 8.02$  and 7.04 ppm, respectively. These chemical shifts are relatively well reproduced with deviations less than 1.01 ppm for H7 and 0.2 ppm for H14 compared to the observed ones. The chemical shifts of the aromatic protons (H11, H22, H24 and H26) appeared as two doublets at  $\delta = 7.19$  and 7.48 ppm. These chemical shifts are relatively well reproduced with deviations less than 0.76 ppm compared to the observed ones. The chemical shifts of the NH protons of pyridazinone appeared as singlet at  $\delta = 10.87$  ppm. Their corresponding one are predicted at  $\delta = 8.39$  ppm.

The carbon NMR spectrum showed the chemical shifts of C9 of carbonyl ( $\text{C}=\text{O}$ ) at  $\delta = 167.67$  ppm. Their corresponding one is obtained at  $\delta = 153.99$  ppm. The signals at  $\delta = 151.26$ , 21.36 and 26.35 ppm are clearly assigned for C23, C21 and C5 carbons of pyridazinone ring. Their corresponding ones are relatively well reproduced with deviations of 13.88, 9.07 and 13.88 ppm, respectively. The signals at  $\delta = 133.80$  and 125.87 ppm are assigned for C6 and C13 carbons of vinyl ( $\text{CH}=\text{CH}$ ) group. These protons are predicted at  $\delta = 118.55$  and 108.06 ppm, respectively. The aromatics carbon chemical shifts of the title compound occurred in the range of 138.52–127.34 ppm. The signals at  $\delta = 20.56$  ppm are assigned for methyl ( $\text{CH}_3$ ) group and their corresponding one is obtained at 12.09 ppm. Generally, the observed and calculated  $^1\text{H}$  and  $^{13}\text{C}$  NMR chemical shifts are in a very good agreement.

### 3.5. UV-vis analysis

The experimental UV-vis absorption spectrum of the title compound was recorded in methanol in the range 200 – 500 nm at 25 °C and has shown in Fig. 4a. The absorption spectrum of (3) is characterized by a longer wavelength band with a maximum around  $\lambda = 324$  nm. The longer wavelength band can be attributed to the  $n \rightarrow \pi^*$  electronic transition resulting from the involved molecular orbitals of the carbonyl ( $\text{C}=\text{O}$ ) and the conjugated  $\pi$  bond of aromatic system [55]. TD-DFT calculations at the B3LYP/6-31+G(d,p) level were performed to obtain information about the excited states and absorption characteristics. The longest wavelength absorption maximum for the title compound is observed in the UV region at  $\lambda = 318$  nm as shown in Fig. 4b. The absorption maximum is assigned to the  $n \rightarrow \pi^*$  transitions that arise from the carbonyl group ( $\text{C}=\text{O}$ ) the conjugated  $\pi$  bond of styryl group of the title compound. The strong cut-off wavelength for the study is 350 nm (Fig. 5b) with an energy band gap of 3.546 eV. The calculated electronic transition (318 nm) is in agreement with the experimental electronic transition observed (324 nm).

### 3.6. Surfaces studies

#### 3.6.1. Hirshfeld surface analysis

Hirshfeld surface analysis was used to quantify the intermolecular contacts of the title compounds, using the software

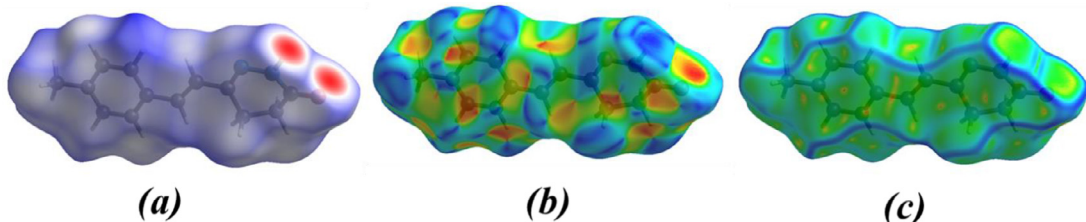


**Fig. 5.** (a)  $d_{\text{norm}}$  mapped on the Hirshfeld surface for visualizing the intermolecular interactions, (b) shape-index map of the title compound and (c) curvedness map of the title compound using a range from  $-4$  to  $4 \text{ \AA}$ .

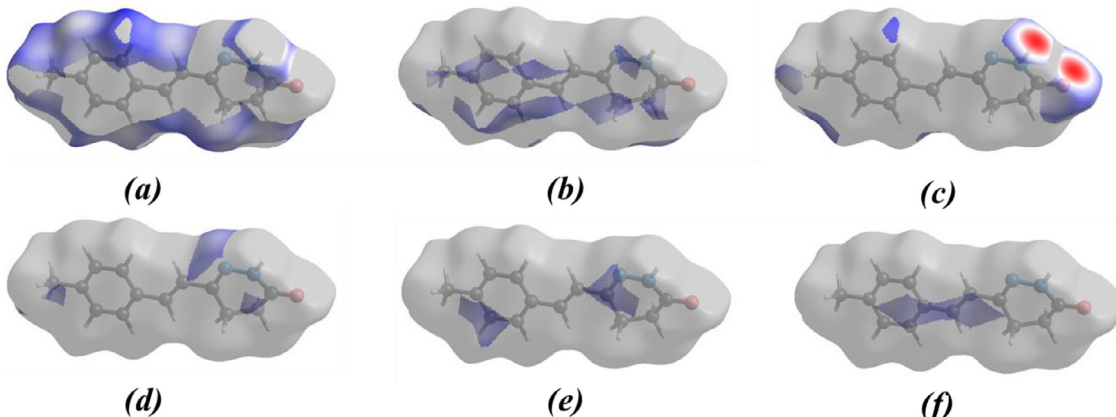


**Fig. 6.** The Hirshfeld surface representations with the function  $d_{\text{norm}}$  plotted onto the surface for (a)  $\text{H} \cdots \text{H}$ , (b)  $\text{H} \cdots \text{C}/\text{C} \cdots \text{H}$ , (c)  $\text{H} \cdots \text{O}/\text{O} \cdots \text{H}$ , (d)  $\text{H} \cdots \text{N}/\text{N} \cdots \text{H}$  interactions.

Crystal-Explorer17.5 [56]. The Hirshfeld surface were planned using a standart (high) surface resolution with the three-dimensional  $d_{\text{norm}}$  surfaces plotted over a fixed color scale of  $-0.5573$  (red) to  $1.3718$  (blue) a.u. The Hirshfeld surfaces of the title compound were mapped over  $d_{\text{norm}}$ , shape index and curvedness **Fig. 5a-c**. The Hirshfeld surface representations with the function  $d_{\text{norm}}$  plotted onto the surface are shown for the  $\text{H} \cdots \text{H}$ ,  $\text{H} \cdots \text{C}/\text{C} \cdots \text{H}$ ,  $\text{H} \cdots \text{O}/\text{O} \cdots \text{H}$ ,  $\text{H} \cdots \text{N}/\text{N} \cdots \text{H}$ ,  $\text{C} \cdots \text{N}/\text{N} \cdots \text{C}$ ,  $\text{C} \cdots \text{C}$  interactions in **Fig. 6a-f**, respectively. The overall two-dimensional fingerprint plot and those delineated into  $\text{H} \cdots \text{H}$ ,  $\text{H} \cdots \text{C}/\text{C} \cdots \text{H}$ ,  $\text{H} \cdots \text{O}/\text{O} \cdots \text{H}$ ,  $\text{H} \cdots \text{N}/\text{N} \cdots \text{H}$ ,  $\text{C} \cdots \text{N}/\text{N} \cdots \text{C}$ ,  $\text{C} \cdots \text{C}$  contacts are illustrated in **Fig. 7a-g**, respectively. The largest interaction is  $\text{H} \cdots \text{H}$  contributing 52.5% to the overall crystal packing. The peak in the center  $d_e = d_i = 1.15 \text{ \AA}$ .  $\text{H} \cdots \text{O}/\text{O} \cdots \text{H}$  contacts makes 14.6% contribution to the Hirshfeld surface. The contacts is represented by a pair of sharp spikes in the region  $d_e + d_i \sim 1.85 \text{ \AA}$  in the fingerprint plot.  $\text{H} \cdots \text{O}/\text{O} \cdots \text{H}$  interactions arises from the intermolecular  $\text{N}-\text{H} \cdots \text{O}$  hydrogen bonding (**Table 2**) and  $\text{H} \cdots \text{O}/\text{O} \cdots \text{H}$  contacts. The contributions of the other contact to the Hirshfeld surface is  $\text{H} \cdots \text{C}/\text{C} \cdots \text{H}$  (19.7%),  $\text{H} \cdots \text{N}/\text{N} \cdots \text{H}$  (8.3%),  $\text{C} \cdots \text{N}/\text{N} \cdots \text{C}$  (2.5%),  $\text{C} \cdots \text{C}$  (2.5%).

### 3.6.2. Molecular electrostatic potentials

Molecular electrostatic potential (MEP) displays molecular size and shape as well as positive, negative and neutral electrostatic potential regions in terms of color grading and is useful in investigating relationships between molecular structure and physico-chemical properties [57,58]. The MEP map (**Fig. 8**) was calculated at the B3LYP/6-31+G(d,p) level of theory. The red and blue-coloured regions indicate nucleophiles (electron rich), and electrophile regions (electron poor), respectively. The white regions indicate neutral atoms. In the title molecule, the red regions are concentrated at the carbonyl group. It possesses the most negative potential and is thus the strongest repulsion site (electrophilic attack). The blue

**Table 6**  
Calculated frontier molecular orbital energies (eV) for 3.

FMO	Energy
$E(\text{HOMO})$	$-6.0709$
$E(\text{LUMO})$	$-1.9986$
$\Delta E (\text{HOMO-LUMO})$	$4.0723$
Hardness, $\eta$	$2.0361$
Softness, $\sigma$	$0.4911$
Electronegativity, $\chi$	$4.0347$

regions indicate the strongest attraction regions, which are occupied mostly by hydrogen atoms.

### 3.7. Frontier molecular orbital analyses

The energy levels for the title compound were computed by theoretically via density functional theory (DFT) using the standard B3LYP functional and 6-31+G(d,p) basis-set calculations [34] as implemented in GAUSSIAN 09 [32]. The HOMO (highest occupied molecular orbital) acts as an electron donor and the LUMO (lowest occupied molecular orbital) as an electron acceptor. When the energy gap is small, the molecule is highly polarizable and has high chemical reactivity. The energy levels, energy gaps, hardness ( $\eta$ ), softness ( $\sigma$ ) and electronegativity ( $\chi$ ) are given in **Table 6**. The electron transition from the HOMO to the LUMO energy level is shown in **Fig. 9**. The chemical hardness and softness of a molecule is a sign of its chemical stability. From the HOMO-LUMO energy gap, we can see whether or not the molecule is hard or soft. If the energy gap is large, the molecule is hard and if small the molecule is soft. Soft molecules are more polarizable than hard ones because they need less energy for excitation. Therefore from **Table 6** we conclude that the title molecule

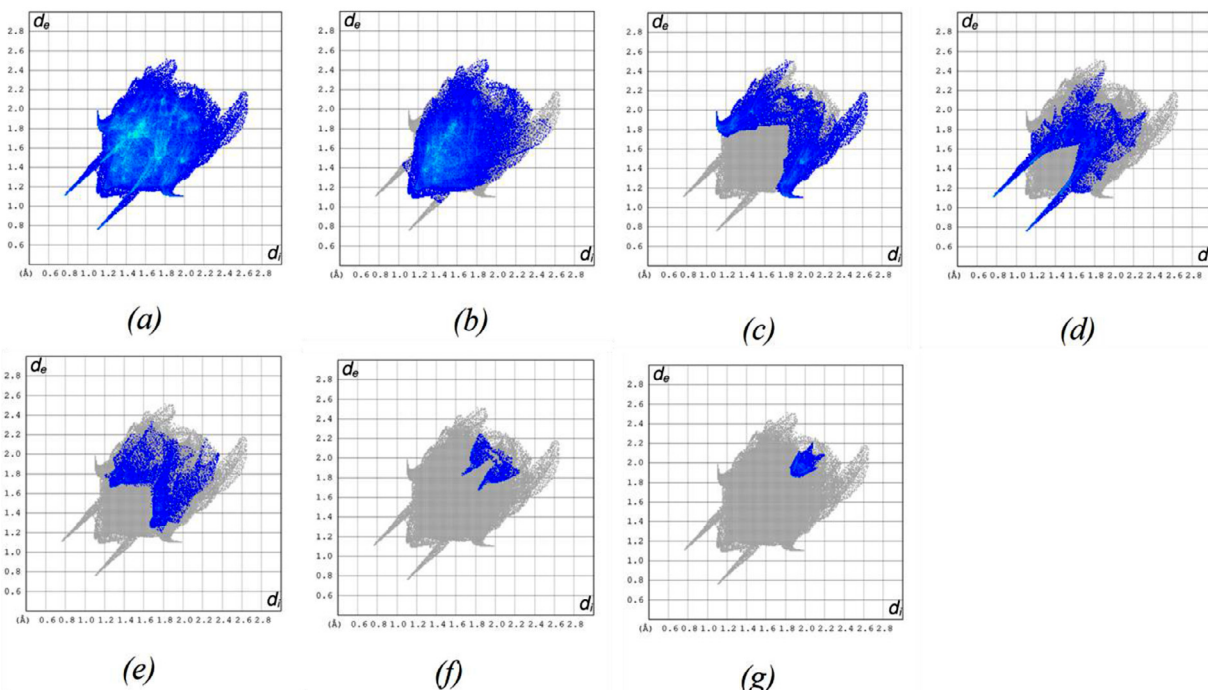


**Fig. 7.** The full two-dimensional fingerprint plots for the title compound, showing (a) all interactions, and delineated into (b) H•••H, (c) H•••C/C•••H, (d) H•••O/O•••H, (e) H•••N/N•••H interactions.

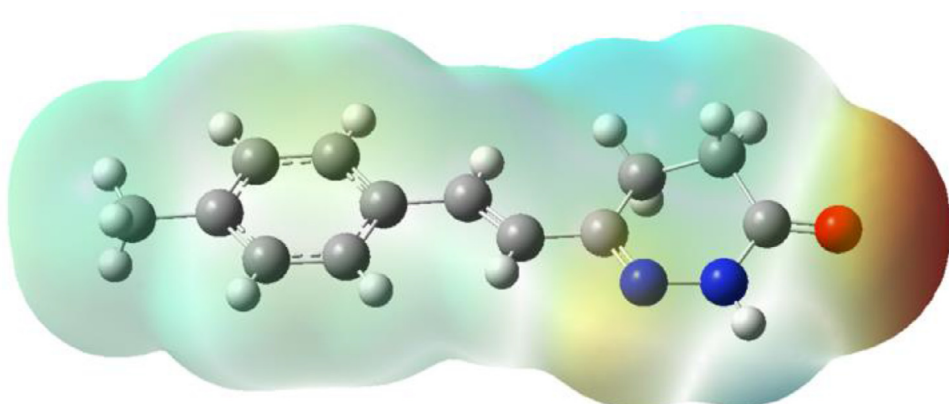


**Fig. 8.** Molecular electrostatic potential surface of **3** in B3LYP/6-31+G (d,p).

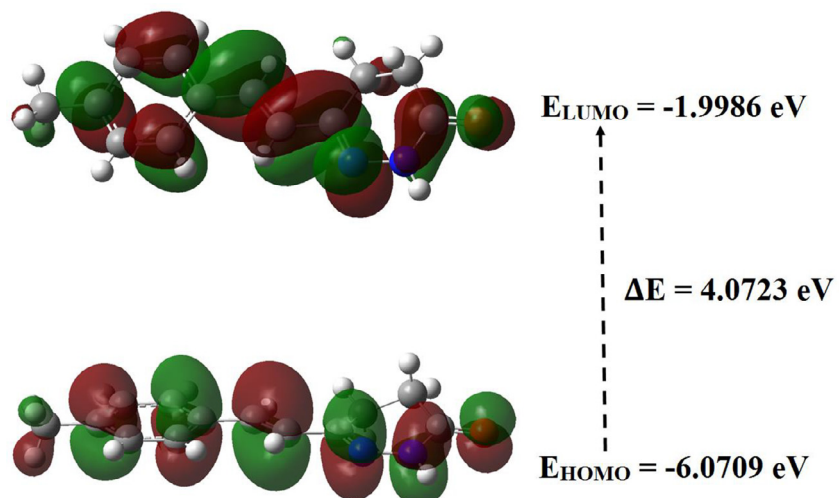


**Fig. 9.** Molecular orbital energy levels of the title compound.

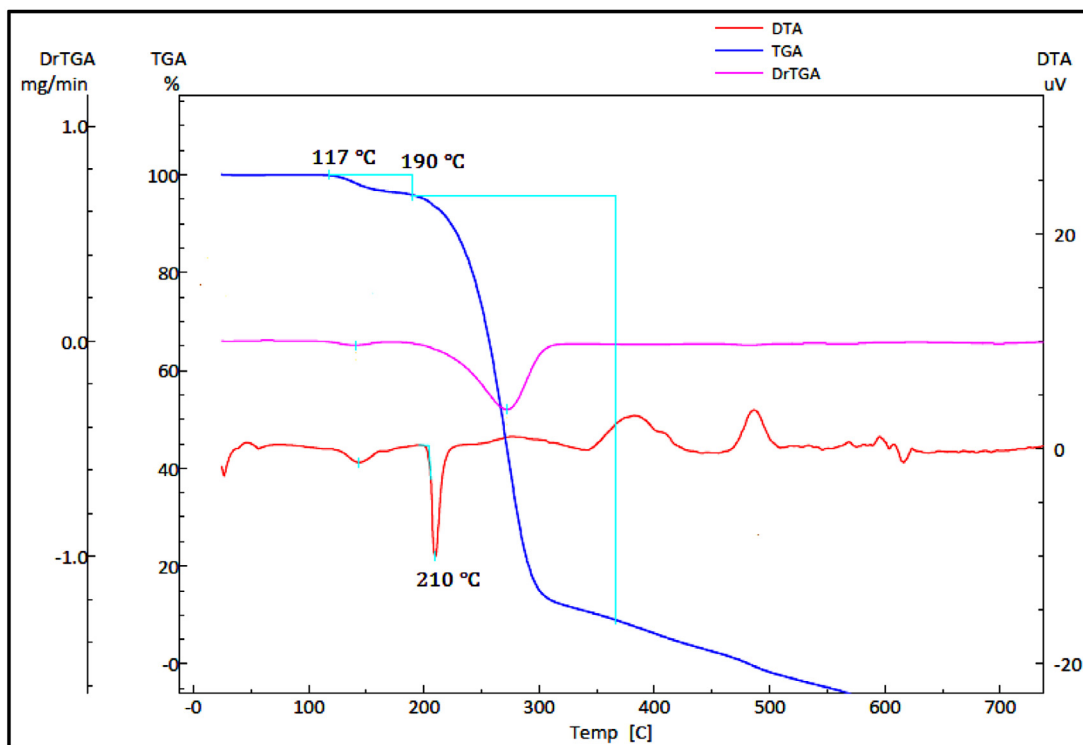


**Fig. 10.** TGA, DrTGA and DTA curves of compound (3).

belongs to the hard materials with a HOMO-LUMO energy gap of 4.0723 eV.

#### 3.8. TGA/DTA thermal analysis

To study the behavior of the sample material against temperature, differential thermal analysis (DTA) and thermogravimetric analysis (TGA) of the compound (**3**) in the temperature range from 50 to 700 °C with a heating rate of 10 °C min<sup>-1</sup>, were studied. Fig. 10 shows the TGA, DrTGA, and DTA curves of compound **3**. The TGA curve of the compound shows two stages of decomposition. The title compound is stable up to 117 °C and then begins to decompose. In the first step of decomposition, the weight loss of 4.067% occurs in the temperature range 117–190 °C. In the second step of decomposition, the weight loss of 86.82% occurs in the temperature range 190–366 °C. The decomposition is completed around 560 °C. In the DTA curve the endothermic peak at 210 °C indicates the melting point of the title compound.

#### 4. Conclusion

A novel pyridazin-3(2H)-one derivative, (*E*)-6-(4-methylstyryl)-4,5-dihydropyridazin-3(2H)-one (**3**) has been synthesized and characterized by FT-IR, UV-vis, <sup>1</sup>H- and <sup>13</sup>C NMR, and single-crystal X-ray diffraction. The electronic structure, FT-IR vibrational frequencies, electronic absorption spectra, chemical shift values have been calculated at DFT/B3LYP with 6-31+G (d,p) basis set. FT-IR spectral analysis indicates that the calculated vibrational frequencies satisfactorily agree with the experimentally assigned values. The TD-DFT calculations lead to a very closer agreement with the experimental absorption spectra. Hirshfeld and MEP surface analyses provide the information concerning the region from where the compound can have intermolecular interactions. The thermal behavior and stability of the title compound were analyzed by using TGA and DTA techniques which revealed that the compound is thermostable up to its melting point.

#### Declaration of Competing Interest

The authors declare that they have no known competing financial interests or personal relationships that could have appeared to influence the work reported in this paper.

#### CRediT authorship contribution statement

**Said Daoui:** Methodology, Investigation. **Cemile Baydere:** Conceptualization, Methodology. **Feride Akman:** Software, Writing - review & editing. **Fouad El Kalai:** Investigation, Resources. **Lhassane Mahi:** Investigation, Resources. **Necmi Dege:** Validation. **Yıldırıay Topcu:** Investigation, Resources. **Khalid Karrouchi:** Conceptualization, Writing - original draft, Writing - review & editing. **Noureddine Benchat:** Supervision.

#### Acknowledgement

This work is supported by Mohammed I University of Oujda and Ondokuz Mayıs University (award project No. PYO.FEN.1906.19.001). Feride Akman would like to thank Bingöl University for the server and Bitlis Eren University for Gaussian software.

#### Supplementary materials

Supplementary material associated with this article can be found, in the online version, at doi:10.1016/j.molstruc.2020.129180.

#### References

- [1] S. Dubey, P.A. Bhosle, Pyridazinone: an important element of pharmacophore possessing broad spectrum of activity, *Med. Chem. Res.* 24 (2015) 3579–3598.
- [2] W. Akhtar, M. Shaquiquzzaman, M. Akhter, G. Verma, M.F. Khan, M.M. Alam, The therapeutic journey of pyridazinone, *Eur. J. Med. Chem.* 123 (2016) 256–281.

- [3] M. Asif, A mini review on biological activities of pyridazinone derivatives as antiulcer, antisecretory, antihistamine and particularly against histamine H3R, *Mini-Rev. Med. Chem.* 14 (2014) 1093–1103.
- [4] M.A. El-Hashash, D.B. Guirguis, N.A.M. AbdEl-Wahed, M.A. Kadhim, Synthesis of novel series of phthalazine derivatives with antibacterial and antifungal evaluation, *J. Chem. Eng. Process Technol.* 5 (2014) 1000191–1000196.
- [5] A.A. Siddiqui, R. Mishra, M. Shaharyar, A. Husain, M. Rashid, P. Pal, Triazole incorporated pyridazinones as a new class of antihypertensive agents: design, synthesis and in vivo screening, *Bioorg. Med. Chem. Lett.* 21 (2011) 1023–1026.
- [6] Y. Boukharsa, B. Meddah, R.Y. Tiendrebeogo, A. Ibrahimi, J. Taoufik, Y. Cherchar, M.E.A. Faouzi, Synthesis and antidepressant activity of 5-[benzo [b] furan-2-ylmethyl]-6-methylpyridazin-3 (2H)-one derivatives, *Med. Chem. Res.* 25 (2016) 494–500.
- [7] D.G.H. Livermore, R.C. Bethell, N. Cammack, A.P. Hancock, M.M. Hann, D.V.S. Green, R.B. Lamont, S.A. Noble, D.C. Orr, *J. Med. Chem.* 36 (1993) 3784–3794.
- [8] C. Barberot, A. Moniot, I. Allart-Simon, L. Malleret, T. Yegorova, M. Laronze-Cochard, J. Sapi, Synthesis and biological evaluation of pyridazinone derivatives as potential anti-inflammatory agents, *Eur. J. Med. Chem.* 146 (2018) 139–146.
- [9] S. Partap, M.J. Akhtar, M.S. Yar, M.Z. Hassan, A.A. Siddiqui, Pyridazinone hybrids: design, synthesis and evaluation as potential anticonvulsant agents, *Bioorg. Chem.* 77 (2018) 74–83.
- [10] T. Wang, Y. Dong, L.C. Wang, B.R. Xiang, Z. Chen, L.B. Qu, Design, synthesis and structure-activity relationship studies of 6-phenyl-4, 5-dihydro-3 (2H)-pyridazinone derivatives as cardiotonic agents, *Arzneimittelforschung* 58 (2008) 569–573.
- [11] M. Tao, L.D. Aimone, J.A. Gruner, J.R. Mathiasen, Z. Huang, J. Lyons, R.L. Hudkins, Synthesis and structure-activity relationship of 5-pyridazin-3-one phenoxypyridines as potent, selective histamine H3 receptor inverse agonists, *Bioorg. Med. Chem. Lett.* 22 (2012) 1073–1077.
- [12] M.A. Dekeyser, Acaricide mode of action, *Pestic. Sci.* 61 (2005) 103–110.
- [13] M. Antifeedant Asif, herbicidal and molluscicidal activities of pyridazinone compounds, *Mini-Rev. Org. Chem.* 10 (2013) 113–122.
- [14] O. Noureddine, S. Gatafaoui, S.A. Brandán, H. Marouani, N. Issaoui, Structural, docking and spectroscopic studies of a new piperazine derivative, 1-Phenylpiperazine-1,4-diium-bis (hydrogen sulfate), *J. Mol. Struct.* 1202 (2020) 127351.
- [15] K. Karrouchi, E. Yousfi, N. Sebbar, Y. Ramli, J. Taoufik, Y. Ouzidan, M. Ansar, Y. Mabkhot, H. Ghabbour, S. Radi, New Pyrazole-Hydrazone Derivatives: x-ray Analysis, Molecular Structure Investigation via Density Functional Theory (DFT) and Their High In-Situ Catecholase Activity, *Int J Mol Sci.* 18 (2017) 2215.
- [16] M.A. Iramain, M.V. Castillo, L. Davies, E. María, M.E. Manzur, S.A. Brandán, Structural and SQMFF study of potent insecticide 4,4-DDT combining the FT-IR and FT-Raman spectra with DFT calculations, *J. Mol. Struct.* 1199 (2020) 126964.
- [17] R.R. Pillai, K. Karrouchi, S. Fettach, S. Armaković, S.J. Armaković, Y. Brik, J. Taoufik, S. Radi, M.E.A. Faouzi, M. Ansar, Synthesis, spectroscopic characterization, reactive properties by DFT calculations, molecular dynamics simulations and biological evaluation of Schiff bases tethered 1, 2, 4-triazole and pyrazole rings, *J. Mol. Struct.* 1177 (2019) 47–54.
- [18] S. Tighadouini, R. Benabbes, M. Tillard, D. Eddike, K. Haboubi, K. Karrouchi, S. Radi, Synthesis, crystal structure, DFT studies and biological activity of (Z)-3-(3-bromophenyl)-1-(1, 5-dimethyl-1 H-pyrazol-3-yl)-3-hydroxyprop-2-en-1-one, *Chem. Cent. J.* 12 (1) (2018) 122.
- [19] O. Noureddine, S. Gatafaoui, S.A. Brandán, A. Sagamaa, H. Marouani, N. Issaoui, Experimental and DFT studies on the molecular structure, spectroscopic properties, and molecular docking of 4-phenylpiperazine-1-ium dihydrogen phosphate, *J. Mol. Struct.* 1207 (2020) 127762.
- [20] K. Karrouchi, S.A. Brandán, Y. Sert, H. El-marzouqi, S. Radi, M. Ferbineteanu, M.E.A. Faouzi, Y. Garcia, M. Ansar, Synthesis, X-ray structure, Vibrational spectroscopy, DFT investigation and biological evaluation studies of (E)-N'-(4-(dimethylamino)benzylidene)-5-methyl-1H-pyrazole-3-carbohydrazide, *J. Mol. Struct.* 1219 (2020) 128541.
- [21] Y. Bouzian, K. Karrouchi, Y. Sert, C.H. Lai, L. Mahi, N.H. Ahabchane, A. Talbaoui, J.T. Mague, E.M. Essassi, Synthesis, spectroscopic characterization, crystal structure, DFT, molecular docking and in vitro antibacterial potential of novel quinoline derivatives, *J. Mol. Struct.* 1209 (2020) 127940.
- [22] R.A. Rudyk, M.A. Checa, C.A.N. Catalán, S.A. Brandán, F.T.-I.R. Structural, FT-Raman and ECD studies on the free base, cationic and hydrobromide species of scopolamine alkaloid, *J. Mol. Struct.* 1180 (2019) 603–617.
- [23] S. Daoui, C. Baydere, T. Chelfi, F. El Kalai, N. Dege, K. Karrouchi, N. Benchat, Polymorphism of 2-(5-benzyl-6-oxo-3-phenyl-1, 6-dihydropyridazin-1-yl) acetic acid with two monoclinic modifications: crystal structures and Hirshfeld surface analyses, *Acta Cryst. E76* (2020) 432–437.
- [24] S. Daoui, E.B. Cinar, F. El Kalai, R. Saddik, K. Karrouchi, N. Benchat, Crystal structure and Hirshfeld surface analysis of 4-(4-methylbenzyl)-6-phenylpyridazin-3 (2H)-one, *Acta Cryst. E75* (2019) 1352–1356.
- [25] S. Daoui, M.S.H. Faizi, F.E. Kalai, R. Saddik, N. Dege, K. Karrouchi, N. Benchat, Crystal structure and the DFT and MEP study of 4-benzyl-2-[2-(4-fluorophenyl)-2-oxoethyl]-6-phenylpyridazin-3 (2H)-one, *Acta Cryst. E75* (2019) 1030–1034.
- [26] S. Daoui, C. Baydere, F. El Kalai, L. Mahi, N. Dege, K. Karrouchi, N. Benchat, Crystal structure, Hirshfeld surface analysis and DFT studies of 2-[5-(4-methylbenzyl)-6-oxo-3-phenyl-1, 6-dihydropyridazin-1-yl] acetic acid, *Acta Cryst. E75* (2019) 1925–1929.
- [27] Bruker, APEX3, SAINT, SADABS & SHELXTL, Bruker AXS, Inc., Madison, WI, 2016.
- [28] G.M. Sheldrick, Crystallographic Shelves: Space-Group Hierarchy Explained, *Acta Cryst. A71* (2015) 3–8.
- [29] G.M. Sheldrick, Crystal structure refinement with SHELXL, *Acta Cryst. C71* (2015) 3–8.
- [30] A.L. Spek, Structure validation in chemical crystallography, *Acta Crystallographica Section D: Biological Crystallography* 65 (2) (2009) 148–155.
- [31] C.F. Macrae, I.J. Bruno, J.A. Chisholm, P.R. Edgington, P. McCabe, E. Pidcock, L. Rodriguez-Monge, R. Taylor, J. van de Streek, P.A. Wood, *Mercury CS2.0* - new features for the visualization and investigation of crystal structures, *J. Appl. Cryst.* 41 (2008) 466–470.
- [32] M.J. Frisch, G.W. Trucks, H.B. Schlegel, G.E. Scuseria, M.A. Robb, J.R. Cheeseman, G. Scalmani, V. Barone, B. Mennucci, G.A. Petersson, H. Nakatsuji, M. Caricato, X. Li, H.P. Hratchian, A.F. Izmaylov, J. Bloino, G. Zheng, J.L. Sonnenberg, M. Hada, M. Ehara, K. Toyota, R. Fukuda, J. Hasegawa, M. Ishida, T. Nakajima, Y. Honda, O. Kitao, H. Nakai, T. Vreven, J.A. Montgomery Jr., J.E. Peralta, F. Ogliaro, M. Bearpark, J.J. Heyd, E. Brothers, K.N. Kudin, V.N. Staroverov, T. Keith, R. Kobayashi, J. Normand, K. RagHAVACHARI, A. Rendell, J.C. Burant, S.S. Iyengar, J. Tomasi, M. Cossi, N. Rega, J.M. Millam, M. Klene, J.E. Knox, J.B. Cross, V. Bakken, C. Adamo, J. Jaramillo, R. Gomperts, R.E. Stratmann, O. Yazev, A.J. Austin, R. Cammi, C. Pomelli, J.W. Ochterski, R.L. Martin, K. Morokuma, V.G. Zakrzewski, G.A. Voth, P. Salvador, J.J. Dannenberg, S. Dapprich, A.D. Daniels, O. Farkas, J.B. Foresman, J.V. Ortiz, J. Cioslowski, D.J. Fox, Gaussian 09, Revision C.01, Gaussian, Inc., Wallingford CT, 2010.
- [33] R. Dennington, T. Keith, J. Millam, GaussView, Version 5, Semichem Inc., Shawnee Mission KS, 2010.
- [34] A.D. Becke, Density-functional exchange-energy approximation with correct asymptotic behavior, *Phys. Rev. A.* 38 (1988) 3098.
- [35] C. Lee, W. Yang, R.G. Parr, Development of the Colle-Salvetti correlation-energy formula into a functional of the electron density, *Phys. Rev. B.* 37 (1988) 785.
- [36] M.H. Jamroz, *Vibrational Energy Distribution Analysis VEDA 4*, Warsaw, 2004.
- [37] Stoe & Cie, X-AREA and X-RED32, Stoe & Cie GmbH, Darmstadt, Germany, 2002.
- [38] S. Abourichaa, N. Benchat, A. Anaflous, A. Melhaoui, T. Ben-Hadda, B. Oussaid, M. Bolte, 6-Phenyl-4, 5-dihydropyridazin-3 (2H)-one, *Acta Cryst. E59* (2003) o802–o803.
- [39] S. Dadou, S. Kansiz, S. Daoui, F. El Kalai, C. Baydere, R. Saddik, K. Karrouchi, N. Dege, N. Benchat, Crystal structures and Hirshfeld surface analyses of 4-benzyl-6-phenyl-4, 5-dihydropyridazin-3 (2H)-one and methyl 2-[5-(2, 6-dichlorobenzyl)-6-oxo-3-phenyl-1, 4, 5, 6-tetrahydropyridazin-1-yl] acetate, *Acta Cryst. E75* (2019) 1679–1684.
- [40] S. Daoui, E.B. Çınar, F. El Kalai, R. Saddik, N. Dege, K. Karrouchi, N. Benchat, Crystal structure, Hirshfeld surface analysis and DFT studies of 6-[((E)-2-(thiophen-2-yl) ethenyl]-4, 5-dihydropyridazin-3 (2H)-one, *Acta Cryst. E75* (2019) 1880–1883.
- [41] S. Daoui, C. Baydere, F. El Kalai, R. Saddik, N. Dege, K. Karrouchi, N. Benchat, Crystal structure and Hirshfeld surface analysis of (E)-6-(4-hydroxy-3-methoxystyryl)-4, 5-dihydropyridazin-3 (2H)-one, *Acta Cryst. E75* (2019) 1734–1737.
- [42] M.A.M. El-Mansy, M.S. El-Bana, S.S. Fouad, On the spectroscopic analyses of 3-Hydroxy-1-Phenyl-Pyridazin-6 (2H) one (HPHP): a comparative experimental and computational study, *Spectrochim. Acta A.* 176 (2017) 99–105.
- [43] S. Bahçeli, H. Gökcé, A Study on Spectroscopic and Quantum Chemical Calculations of Levosimendan, *Indian. J. Pure. Ap. Phys.* 52 (2014) 224–235.
- [44] D.W. Mayo, F.A. Miller, R.W. Hannah, Course Notes On the Interpretation of Infrared and Raman spectra, John Wiley & Sons, 2004.
- [45] K. Karrouchi, S. Fettach, M.M. Jotani, A. Sagamaa, S. Radi, H.A. Ghabbour, Y.N. Mabkhot, B. Himmi, M.E.A. Faouzi, N. Issaoui, Synthesis, crystal structure, hirshfeld surface analysis, DFT calculations, anti-diabetic activity and molecular docking studies of (E)-N'-(5-bromo-2-hydroxybenzylidene) isonicotinohydrazide, *J. Mol. Struct.* 1221 (2020) 128800.
- [46] S. Bahçeli, H. Gökcé, A Study on Spectroscopic and Quantum Chemical Calculations of Levosimendan, *Indian. J. Pure. Ap. Phys.* 52 (2014) 224–235.
- [47] S.M. Soliman, J. Albering, M.A. Abu-Youssef, Molecular structure, spectroscopic properties, NLO, HOMO-LUMO and NBO analyses of 6-hydroxy-3 (2H)-pyridazinone, *Spectrochim. Acta A.* 136 (2015) 1086–1098.
- [48] O. Noureddine, S. Gatafaoui, S.A. Brandán, H. Marouani, N. Issaoui, Structural, docking and spectroscopic studies of a new piperazine derivative, 1-Phenylpiperazine-1,4-diium-bis (hydrogen sulfate), *J. Mol. Struct.* 1202 (2020) 127351.
- [49] S. Gatafaoui, N. Issaoui, S.A. Brandán, T. Roisnel, H. Marouani, Synthesis and characterization of p-xylylenediaminiumbis(nitrate). Effects of the coordination modes of nitrate groups on their structural and vibrational properties, *J. Mol. Struct.* 1151 (2018) 152–168.
- [50] O. Noureddine, S. Gatafaoui, S.A. Brandán, A. Sagamaa, H. Marouani, N. Issaoui, Experimental and DFT studies on the molecular structure, spectroscopic properties, and molecular docking of 4-phenylpiperazine-1-ium dihydrogen phosphate, *J. Mol. Struct.* 1207 (2020) 127762.
- [51] S.R. Sheeqa, N.A. Mangalam, M.P. Kurup, Y.S. Mary, K. Raju, H.T. Varghese, C.Y. Panicker, Vibrational spectroscopic studies and computational study of quinoline-2-carbaldehyde benzoyl hydrazone, *J. Mol. Struct.* 973 (2010) 36–46.
- [52] B. Dede, D. Avci, S. Bahçeli, Study on the 4-ethoxy-2-methyl-5-(4-morpholinyl)-3 (2H)-pyridazinone using FT-IR, <sup>1</sup>H and <sup>13</sup>C NMR, UV-vis spectroscopy, and DFT/HSE1PBE method, *Can. J. Phys.* 96 (9) (2018) 1042–1052.

- [53] H. Gökce, S. Bahçeli, Spectroscopic and quantum chemical studies on bromopyrazone, *Spectrochim Acta A* 133 (2014) 741–751.
- [54] M.A.M. El-Mansy, M.S. El-Bana, S.S. Fouad, On the spectroscopic analyses of 3-Hydroxy-1-Phenyl-Pyridazin-6 (2H) one (HPHP): a comparative experimental and computational study, *Spectrochim. Acta A* 176 (2017) 99–105.
- [55] M. Pokharia, S.K. Yadav, H. Mishra, N. Pandey, R. Tilak, S. Pokharia, Synthesis, spectroscopic characterization, biological activity and theoretical studies of (E)-N3-(2-chlorobenzylidene)-H-1, 2, 4-triazole-3, 5-diamine, *J. Mol. Struct.* 1144 (2017) 324–337.
- [56] M.J. Turner, J.J. McKinnon, S.K. Wolff, D.J. Grimwood, P.R. Spackman, D. Jayatilaka, M.A. Spackman, *CrystalExplorer17*, University of Western Australia, 2017 <http://hirshfeldsurface.net>.
- [57] J.S. Murray, K. Sen, *Molecular Electrostatic potentials: Concepts and Applications*, Elsevier, 1996.
- [58] E. Scrocco, J. Tomasi, *Advances in Quantum Chemistry*, Academic Press, New York, 1978.